

# Fundamental Study of Aerodynamic Drag Reduction for Vehicle with Feedback Flow Control\*

Keisuke NISUGI\*\*, Toshiyuki HAYASE\*\*\* and Atsushi SHIRAI\*\*\*

The present paper deals with a fundamental study of aerodynamic drag reduction for a vehicle with a feedback flow control. As the first step, two-dimensional calculation was performed for a flow around a simplified vehicle model. The mechanism of unsteady drag was investigated in relation to the vortex shedding from the model. The location of the control flow nozzle was so determined that the control flow influences the drag most effectively. The key in designing the present feedback control is the definition of the output signal. Based on the physical consideration of the drag generation, the location of the output velocity measurement was changed within a limited region near the front windshield. A systematic calculation revealed that the output signal defined in a small region results in a significant drag reduction of 20% with respect to the case without control. The present feedback flow control is generally applicable to the drag reduction of the bluff body for which the drag is generated under the same mechanism of essentially two-dimensional vortex shedding.

**Key Words:** Numerical Simulation, Feedback Flow Control, Vehicle, Drag Reduction, Vortex Shedding, Pressure Drag

## 1. Introduction

Aerodynamic drag is crucial for a vehicle's mileage especially at high speeds as it increases in proportion to the square of the vehicle velocity<sup>(1)</sup>. Conventionally, aerodynamic drag has been reduced by designing a body shape. Lay pointed out the importance of streamlining the body shape through wind tunnel experiments<sup>(2)</sup>, while Hucho et al. reported the effect of the body detail<sup>(3)</sup>. Recently computational fluid dynamics (CFD) has been applied to the aerodynamic design of body shape. Wake has been reported as an important factor of a vehicle's performance<sup>(4)</sup>. Since the magnitude of the drag depends on the flow field around the body, it can be reduced not only by changing the body shape but also by directly changing the flow field. In the viewpoint of the flow control, design of the body shape is classified as a passive flow control. Another method of the flow control for aerodynamic drag reduction is desired in order to increase freedom of design

to allow comfortable spacing while attaining further drag reduction.

Many studies have examined flow field control, for example, by methods such as separation control by boundary layer suction, or drag reduction via riblets or polymer addition<sup>(5)</sup>. A number of studies have examined feedback flow control techniques. Choi et al.<sup>(6)</sup> numerically simulated a channel flow, revealing the suppression of turbulent fluctuation, and an associated drastic reduction in drag, due to local manipulation of the flow via actuators distributed along the channel wall. Lumley et al.<sup>(7)</sup> reported the physical basis of feedback control and a low-dimensional model for a comparatively simple turbulent flow. Recently Bewley et al.<sup>(8)</sup> made a theoretical work on a robust control of flow modeled as an infinite dimensional and nonlinear dynamical system. However, these studies treat fundamental flow problems of simple geometry. Few studies have examined the feedback control of a flow over shapes having complex geometry of practical importance, such as that over a vehicle.

The present study concerns the aerodynamic drag reduction of a vehicle by the feedback flow control. The concept of the flow control is illustrated in Fig. 1. Sensors mounted on a vehicle provide the controller with the flow information, such as velocity components or pressure. Based on this flow information the controller produces the

\* Received 3rd June, 2003 (No. 03-4081)

\*\* Graduate School of Information Science, Tohoku University, 2-1-1 Katahira, Aoba-ku, Sendai, Miyagi 980-8577, Japan

\*\*\* Institute of Fluid Science, Tohoku University, 2-1-1 Katahira, Aoba-ku, Sendai, Miyagi 980-8577, Japan.  
E-mail: hayase@ifs.tohoku.ac.jp

control signal which drives the actuator. The actuator applies the blowing or suction of the fluid through the control port in order to change the flow field. Feedback control generally has several advantages to feed forward control<sup>(9)</sup>. Many sophisticated feedback control techniques have been developed in control theory<sup>(9)</sup>, but few of them is applicable to real flow control problems.

As a fundamental consideration, the present paper deals with a simplest problem of the feedback control of a two-dimensional flow around a vehicle. Three-dimensional effects, such as rolled-up vortices along the rear deck<sup>(10)</sup>, and quantitative evaluation of turbulent flow are ignored in the present study. In a previous work<sup>(11)</sup>, we performed a numerical simulation pointing out the possibility of drag reduction with a feedback flow control. However, details of the flow control including the mechanism of the drag reduction have not been clarified. The present paper carries out numerical analysis in order to give a physical explanation for the drag reduction with the feedback flow control.

### Nomenclatures

- $dF, d\Pi$  : change rate of time-averaged drag and power consumption, respectively  
 $F$  : Drag  
 $F_{avg}, F_{0avg}$  : Time-averaged drag with and without control, respectively  
 $K_g$  : Gain  
 $L^*$  : Vehicle height (reference length)  
 $P$  : Pressure  
 $\mathbf{P}_m$  : Monitoring point  
 $Re_0$  : Reynolds number ( $= U^* L^* / \nu^*$ )  
 $t$  : Time  
 $U^*$  : Vehicle velocity (reference velocity)  
 $u, v$  : Velocity component in  $x, y$  direction, respectively  
 $v_a, v_{blow}, v_m$  : Bias velocity, control flow velocity and velocity at monitoring point, respectively  
 $W^*$  : Vehicle's width  
 $x_{wall}$  : Distance along the body surface measured clockwise from the front lower end (Fig. 5)  
 $(x, y)$  : Cartesian coordinate system  
 $\Pi^*, \Pi_0^*, \Pi_{blow}^*$  : Power required to compensate for aero-

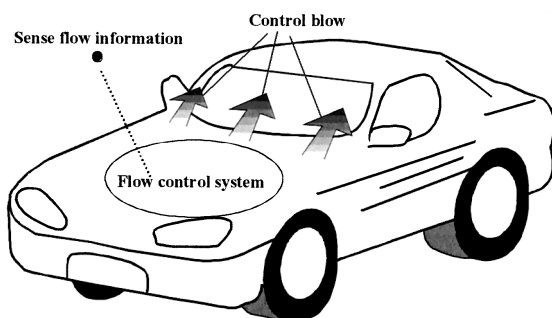


Fig. 1 Concept of the feedback flow control of the vehicle

dynamic drag with and without control and to give control flow, respectively

$\nu^*$  : Kinematic viscosity

$\rho^*$  : Density of fluid

Superscript

\* : Dimensional value

### 2. Formulation

The geometry for the present numerical simulation is shown in Fig. 2. A simple two-dimensional model is treated herein, because the present study focuses on the fundamental understanding of the aerodynamic drag reduction by feedback flow control. Solid walls are placed in the upper and lower boundary, for the sake of convenience in specifying the boundary condition. The distance between the upper wall and the vehicle is set large enough to eliminate unfavorable effects from the wall. Dimensions of the present model are given in Table 1.

Incompressible viscous fluid is assumed in the calculation. The governing equations are the Navier-Stokes equation and the equation of continuity in dimensionless form:

$$\begin{cases} \frac{\partial \mathbf{u}}{\partial t} + (\mathbf{u} \cdot \text{grad}) \mathbf{u} = -\text{grad } p + \frac{1}{Re_0} \nabla^2 \mathbf{u} \\ \text{div } \mathbf{u} = 0 \end{cases} \quad (1)$$

Dimensionless values are defined using the vehicle height  $L^*$ , the vehicle velocity  $U^*$ , and the density  $\rho^*$ . As given in Table 1, we assume the velocity  $U^*$  as 30.24 m/s

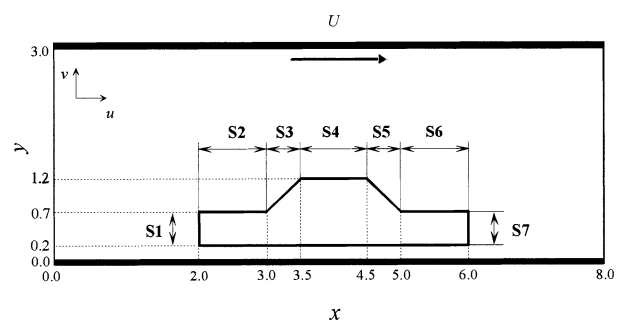


Fig. 2 Geometry and coordinate system

Table 1 Computational condition

$A^*$	Area of control flow port	0.075 m <sup>2</sup>
$L^*$	Vehicle height (reference length)	1.0 m
$Re_0$	Reynolds number ( $U^* L^* / \nu^*$ )	$2.02 \times 10^6$
$U^*$	Vehicle velocity (reference velocity)	30.24 m/s (100km/h)
$W^*$	Vehicle width	1.5 m
$\nu^*$	Kinematic viscosity	$15.0 \times 10^{-6}$ m <sup>2</sup> /s (20°C, air)
$\rho^*$	Density of fluid (reference)	1.205 kg/m <sup>3</sup> (20°C, air)
$\Delta h$	Grid spacing	0.05
$\Delta t$	Time step	0.1
$\epsilon$	Total residual at convergence	0.045
	CPU time for one time step	14.98 s (Origin 2000)

(100 km/h) and the corresponding Reynolds number as  $2.02 \times 10^6$ . A three-dimensional turbulent flow analysis is necessary for quantitative evaluation of the relevant flow of such a high Reynolds number. However, a simple two-dimensional flow model without a turbulence model is employed here in considering the objective of this work to understand the fundamental mechanism of drag reduction by modifying the large flow structure through the feedback flow control. The Cartesian coordinate system is fixed on the vehicle, which moves in the negative  $x$ -direction. In this case, the upper and the lower walls move in the positive  $x$ -direction at velocity  $U^*$ . A parallel flow with a uniform velocity  $U^*$  is applied as the upstream boundary condition. The downstream boundary condition is defined as free stream flow ( $\partial/\partial x = 0$ ). The non-slip condition is assumed for the solid walls.

A simple explanation of the numerical method is given here. A uniformly spaced staggered grid system is defined. The discretized representations of the governing equations are obtained through the control volume method and are solved using an algorithm that is similar to the SIMPLER method<sup>(12)</sup>. In particular, convective terms are discretized via consistently reformulated QUICK scheme<sup>(13)</sup>, and time derivative terms are discretized via second-order implicit scheme<sup>(14)</sup>.

The feedback control is described here. As the output signal, the monitoring velocity  $v_m$ , the velocity in the  $y$ -direction at the monitoring point  $\mathbf{P}_m$ , is measured in the flow field. The input signal is the velocity of the flow in the  $y$ -direction,  $v_{blow}$ , given at the control port on the vehicle body. A simple proportional control is applied here. The control flow velocity  $v_{blow}$  is determined according to the following formula:

$$v_{blow} = K_g(v_m - v_a), \quad (2)$$

where  $v_a$  is the bias velocity and  $K_g$  is the feedback gain. Details of the feedback control scheme are described later.

The drag is obtained by integrating the pressure and the shear stress along the surface of the vehicle. In the following, the drag reduction by the feedback control is evaluated using the change rate of drag  $dF$ , which is defined as

$$dF = \frac{F_{avg} - F_{0avg}}{F_{0avg}} \times 100 \quad (\%), \quad (3)$$

where  $F_{avg}$  and  $F_{0avg}$  are the time-averaged drag with and without control, respectively. The change rate of power  $d\Pi$  is obtained as the total power change, including the control flow as

$$d\Pi = \frac{(\Pi^* + \Pi_{blow}^*) - \Pi_0^*}{\Pi_0^*} \times 100 \quad (\%), \quad (4)$$

where  $\Pi^*$  and  $\Pi_0^*$  are the power required to compensate for aerodynamic drag with and without control, respectively, and  $\Pi_{blow}^*$  is the power consumption for the control flow calculated as

$$\Pi_{blow}^* = \frac{1}{2} \rho^* |v_{blow}^*|^3 |A^*|. \quad (5)$$

### 3. Results and Discussions

In this section, the accuracy of the numerical simulation is first verified. Then the relationship between the flow field and the drag is investigated with and without control.

The accuracy of numerical simulation depends heavily on the grid spacing  $\Delta h$  (same value in both  $x$ - and  $y$ -directions) and the time step  $\Delta t$ . Test calculations were performed for three grid spacings and several time steps. Figure 3 shows the convergence of the time-averaged drag with the time step and the grid spacing. For each grid spacing, the time-averaged drag converges with decreasing time step. Comparison among the convergent values reveals that relatively fine grids of  $\Delta h = 0.025$  and  $0.05$  yield almost identical results, whereas the coarse grid of  $\Delta h = 0.1$  yields a larger result. The error between the result obtained using  $\Delta h = 0.025$ ,  $\Delta t = 0.01$  and that obtained using  $\Delta h = 0.05$ ,  $\Delta t = 0.1$  is 7%. Considering both the accuracy and the computational time, the following calculations were all performed using the grid spacing  $\Delta h = 0.05$  and the time step  $\Delta t = 0.1$ . The computational condition is summarized in Table 1.

#### 3.1 Relation between flow field and drag without control

The time dependent calculation was performed for the flow field around the vehicle without control with the initial condition of null velocity. After some transient time, unsteady flow with repetitive vortex shedding and corresponding drag force fluctuation were obtained as shown in Fig. 4. The insets in Fig. 4 show the drag variation with time. In Fig. 4(a), the flow is separated from the leading edge of the roof (denoted by an arrow), and several vortices of almost the same scale exist behind the rear window. At the next time step, shown in Fig. 4(b), these

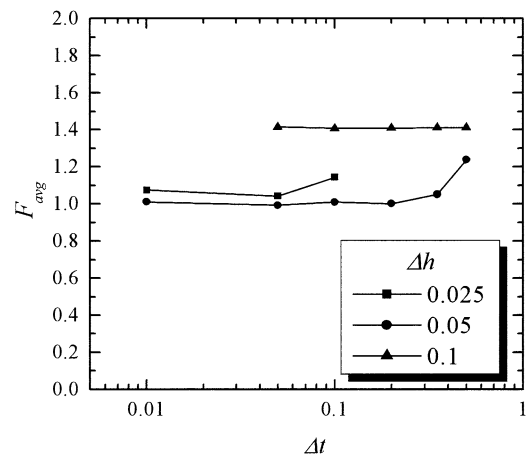


Fig. 3 Grid convergence of numerical solution

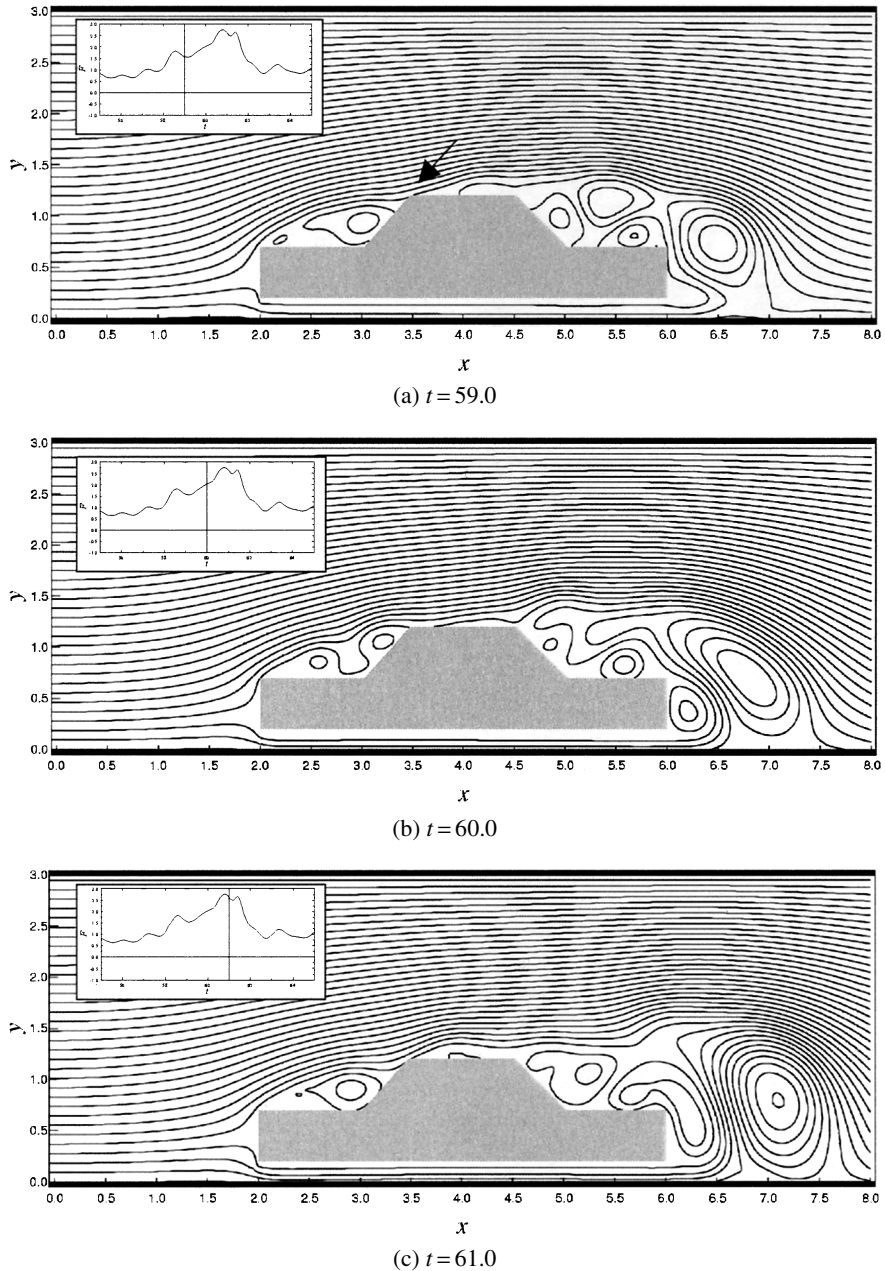


Fig. 4 Flow field without control

vortices merge to generate a relatively large vortex that separates behind the vehicle. In Fig. 4 (c), which corresponds to the highest drag condition, a large vortex separates from the rear-deck and moves downstream, while secondary vortices at S6 and S7 (see Fig. 2) merge into a single vortex.

Aerodynamic drag consists of the pressure drag and the friction drag. The present paper, however, focuses on the pressure drag since the pressure drag usually dominates for the flow around bluff bodies. The pressure distribution along the vehicle surface is plotted in Fig. 5 for the high-drag case (corresponding to Fig. 4 (c)), the low-drag case and the time-averaged result. In the figure, the abscissa represents the distance along the surface of the vehi-

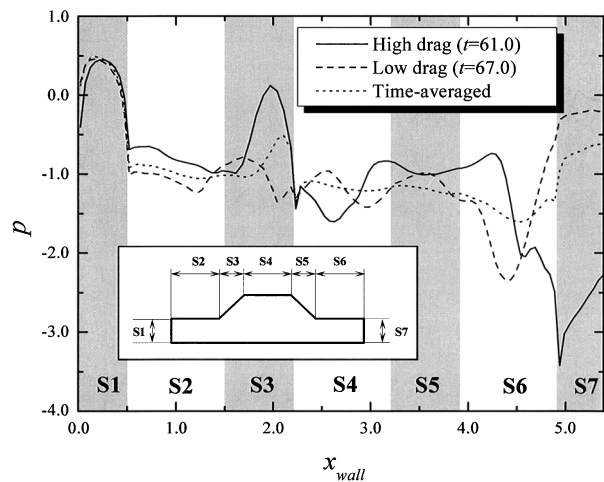


Fig. 5 Pressure distribution without control

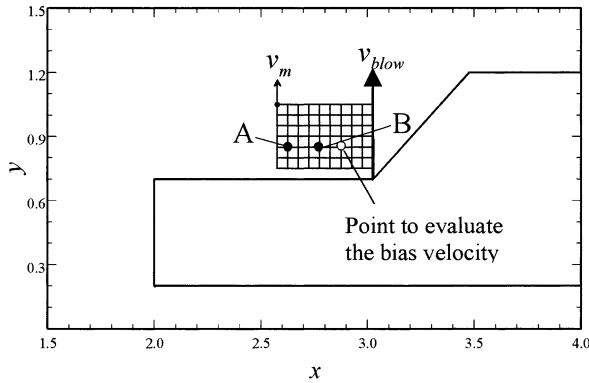


Fig. 6 Schematic of feedback control

cle as measured from the lower-front corner (see the insert at the lower-left of the figure). Pressure drag is produced by panels S1, S3, S5, and S7 (hatched area in Fig. 5). The pressure distributions reveal that for the high-drag case, represented by the solid line, relatively high pressure is produced on S3 and low pressure is produced on S7, both of which contribute to increased drag. The flow field in Fig. 4 and the pressure distribution in Fig. 5 indicate that the low-pressure area at S7 is due to the large vortex behind the vehicle. Since the pressure drag is closely related to vortex structure, the feedback control was applied in an attempt to modify the vortex structure by applying the control flow.

**3.2 Feedback flow control design**

The feedback control is designed here. The location of the control port has been determined from former simulation results with a constant blowing or suction through the control port at several locations on the vehicle<sup>(10)</sup>. The most significant effect on the time-averaged drag appeared in the case that the control port was located at the bottom of the front windshield, as shown in Fig. 6. It was found that small vortices, which separated from the leading edge of panel S4, merged to generate a large scale vortex behind the vehicle. Blowing or suction through this control port possibly control the flow separation at the leading edge of panel S4, which is a source of the large-scale vortices behind the vehicle. The location of the control port was thus set at this location.

In the followings, we determine the parameters in the control law defined in Eq. (2): the monitoring point  $\mathbf{P}_m$ , the bias velocity  $v_a$ , and the feedback gain  $K_g$ . First, the effect of the location of the monitoring point  $\mathbf{P}_m$  is investigated. Since the present paper intends to reduce the drag by controlling the vortex flow over the vehicle surface, the monitoring point determining the control flow is assumed in a limited region with the size similar to the vortex at the location upstream of the control port. Numerical simulation was performed using the feedback gain  $K_g = 1.0$ , and the bias velocity  $v_a = 0.13$  (time-averaged velocity without control at the point (2.875, 0.85) located one third in hor-

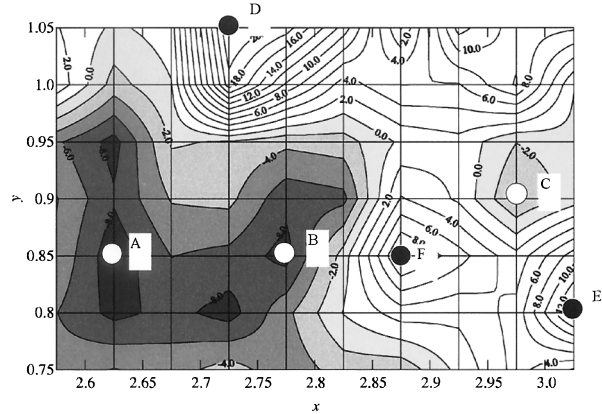


Fig. 7 Change rate of drag with monitoring point ( $v_a = 0.13$ ,  $K_g = 1.0$ )

izontal and vertical direction from the lower right corner of the region, see Fig. 6) at 70 different monitoring points in the range  $2.575 \leq x \leq 3.025$  and  $0.75 \leq y \leq 1.05$  at intervals of 0.05. The monitoring points correspond to the grid points in Fig. 6.

Figure 7 shows the contour for the change rate of the time-averaged drag  $dF$  (%) as a function of the location of the monitoring point  $\mathbf{P}_m$ . The control effect heavily depends on the monitoring point. A negative drag change, corresponding to the drag reduction, was attained at 37 points of the total 70 points (shaded area in Fig. 7). Characteristic points **A**, **B**, and **C**, denoted by open symbols, represent drag reduction and **D**, **E**, and **F**, denoted by closed symbols, represent increases in drag. The largest drag reduction of 9% was achieved at the monitoring points **A** and **B**.

The variations in the drag and the control flow are presented in Fig. 8 for the cases using several characteristic monitoring points. The figures of the left-hand side correspond to the drag and those of the right-hand side correspond to the control flow velocity. All of the control flows are nearly periodical. Peak frequencies of the variations of the drag and the control flow are the same for the cases with monitoring points **A** and **B**, corresponding to drag reduction. It is also noted that the averaged control flows in the cases of **A** and **B** are negative (suction).

In the following, the effect of the other control parameters on drag reduction is determined using the monitoring point **A** or **B**. The effect of the feedback gain is investigated for the cases with monitoring point **A** and **B** in Fig. 9. All the feedback gain values used in this study show the drag reduction (negative drag change). For the case of the monitoring point **B**, the largest drag reduction of 25% is accomplished at the feedback gain of 1.2, but such a drag reduction is very sensitive to the gain. The drag reduction over 15% is obtained for the feedback gain in the range of 1.25 – 1.4. For the monitoring point **A**, the drag reduction effect increased in accordance with the in-

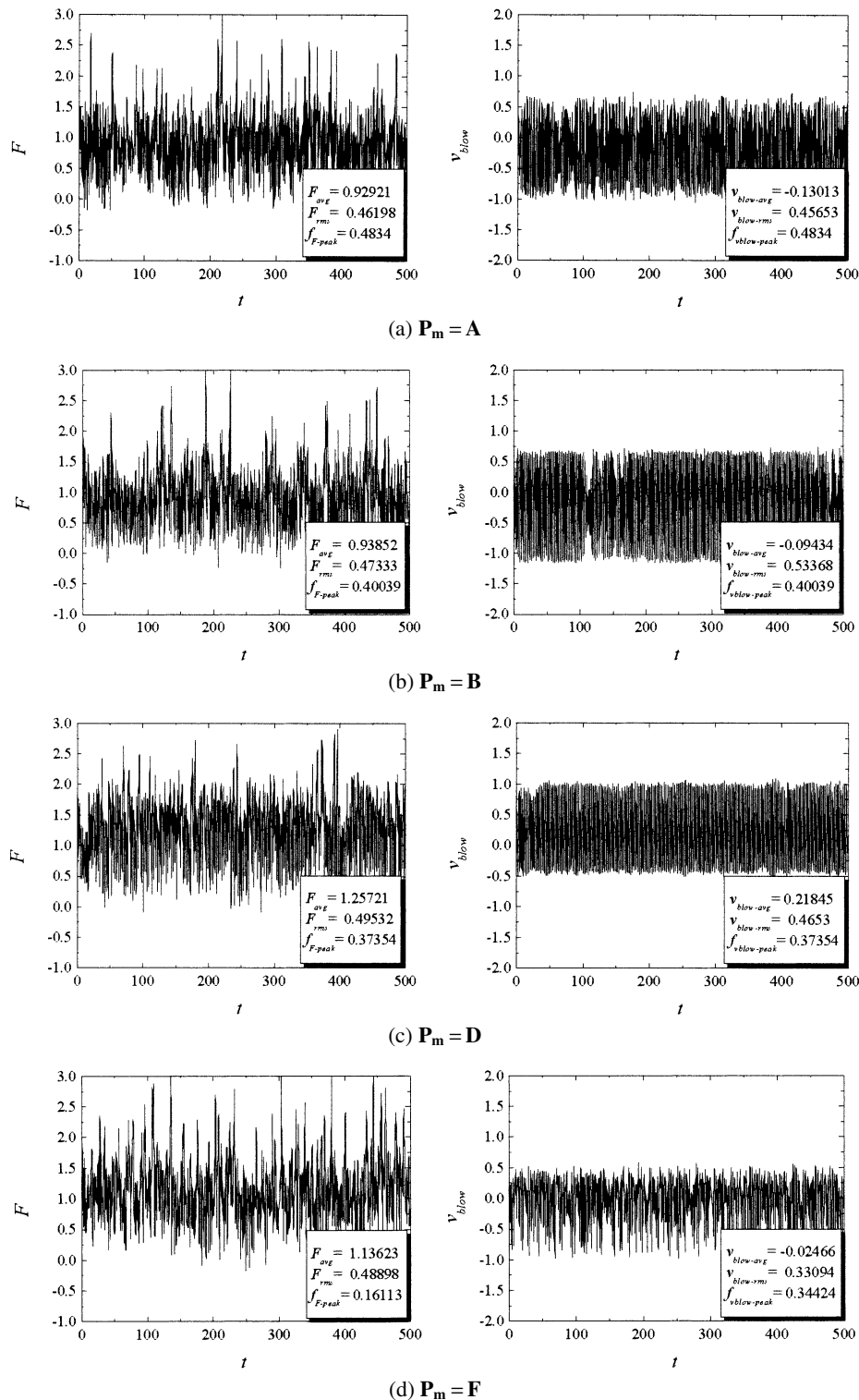


Fig. 8 Control results for characteristic monitoring points ( $v_d = 0.13$ ,  $K_g = 1.0$ ). The left-hand side represents drag, and the right-hand side represents control flow.

crease of the feedback gain. The drag reduction over 15% is obtained for the feedback gain larger than 2.0. However, such a large gain results in a large energy consumption for the control flow. Overall energy saving is not achieved for the gain larger than 2.0. Based on the above results, the monitoring point is fixed at **B** and the gain is fixed to 1.3.

The effect of the bias velocity is shown in Fig. 10. Bias velocity larger than 0.07 accomplishes a drag reduction, while negative bias velocity results in large drag increasing. In particular, a bias velocity around 0.12 shows a drag reduction more than 20%. The upper-right inset shows the result in this range. The drag reduction dras-

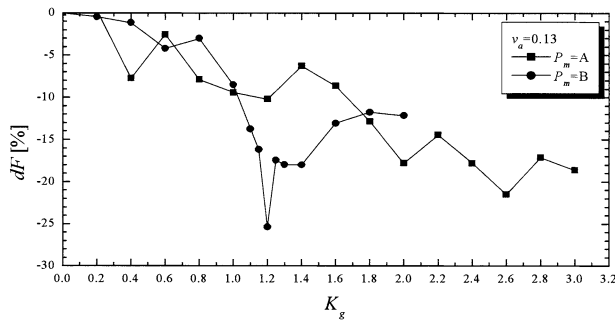


Fig. 9 Change rate of drag with feedback gain using monitoring point A or B ( $v_a = 0.13$ )

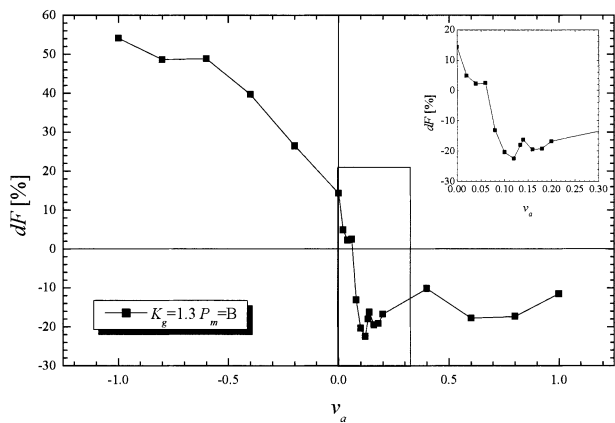


Fig. 10 Change rate of drag with bias velocity ( $K_g = 1.3$ ,  $P_m = B$ )

tically increases at the bias velocity of 0.06 and keeps a large value in the range of 0.1–0.2. Therefore, the bias velocity is fixed to 0.12 in the followings.

We summarize the parameter set determined in the above argument for the feedback flow control in Eq. (2).

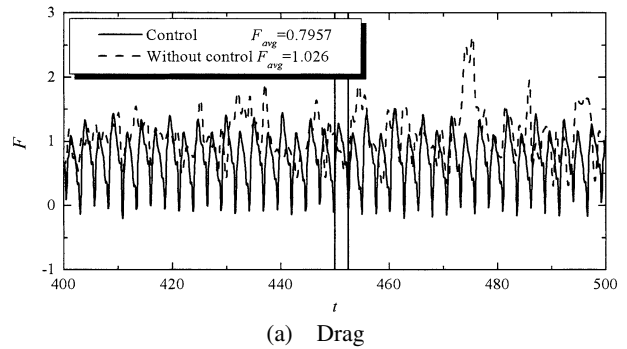
$$\begin{aligned}
 &\text{Monitoring point: } P_m = B \\
 &\text{Feedback gain: } K_g = 1.3 \\
 &\text{Bias velocity: } v_a = 0.12
 \end{aligned} \tag{6}$$

It should be noted that the parameter set whose value is adjusted independently does not necessarily accomplish the optimum (largest) drag reduction over the present parameter range. However, the drag reduction of the present parameter set is possibly close to the optimum one, since the sensitivity of the parameters to the drag reduction is sufficiently small.

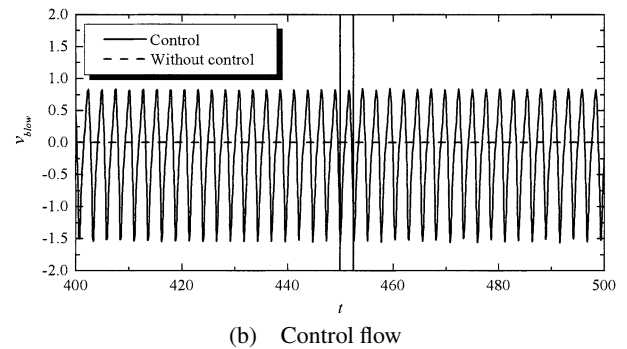
### 3.3 Flow control results

This section describes a result of the flow control with the parameter set in Eq. (6) in comparison with the standard result without control. Variations of the drag and the control flow are plotted in Fig. 11 (a) and (b), respectively. The fluctuation of the drag is periodical for the result with the flow control, but is not for the one without control (Fig. 11 (a)). The control flow velocity in Fig. 11 (b) is also periodic and synchronizes with the drag variation.

In order to investigate the mechanism of the drag re-



(a) Drag



(b) Control flow

Fig. 11 Results of feedback flow control ( $P_m = B$ ,  $v_a = 0.12$ ,  $K_g = 1.3$ )

duction, variation of the flow structure is investigated. Figure 12 shows the sequence of the flow field over one cycle of the periodic drag variation (between the two vertical lines in Fig. 11). The insets at upper-left show the drag with a solid line and the control flow velocity with a dashed line for approximately four cycles of oscillation. The vertical line in the insets represents the time at which the flow field is presented. Two arrows ahead of and at the lower edge of the front windshield represent the monitoring velocity and the control flow velocity, respectively. In Fig. 12 (a), the center of the vortex locates at the monitoring point B, so the monitoring velocity is approximately 0 and the control flow velocity is very small. From this time to the next time in Fig. 12 (b), the vortex moves downstream and increasing positive velocity appears at the monitoring point, resulting in increase of the blowing control flow. The vortex is pushed up by the blowing control as illustrated in Fig. 12 (b). As the next vortex generated from the leading edge of S2 panel approaches to the monitoring point, the blowing control flow is changed to the suction flow as shown in Fig. 12 (c). The suction control flow weakens the pushed-up vortex and strengthens the approaching vortex. In the next time, the strengthened vortex reaches the same position as illustrated in Fig. 12 (a). This process is periodically repeated due to the feedback flow control. Vortices are carried downstream over the front windshield and along the surface of the S4 panel contributing to the generation of a small vortex on the upper part of the rear windshield (S5) (Fig. 12 (a)). The vortex expands

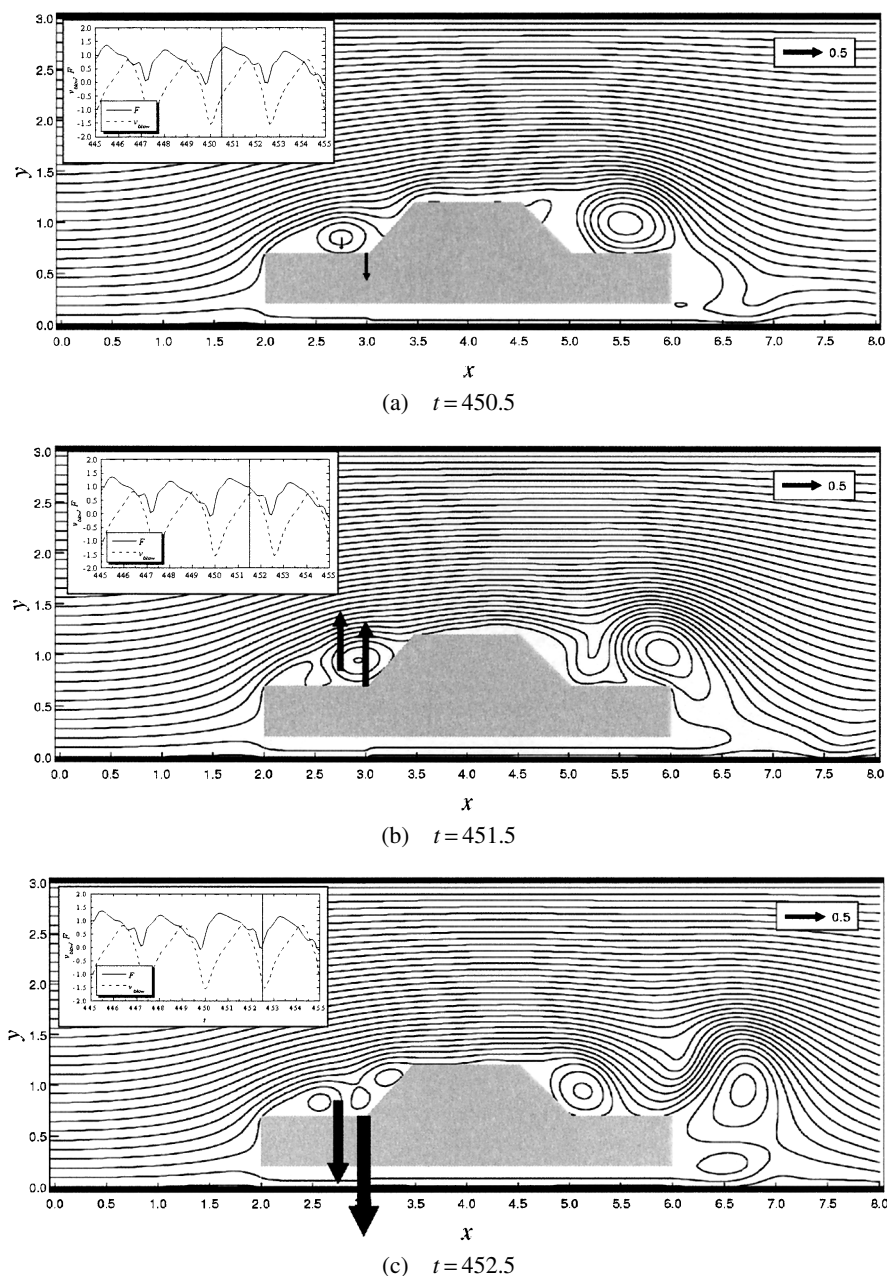


Fig. 12 Flow field with feedback control ( $\mathbf{P}_m = \mathbf{B}$ ,  $v_a = 0.12$ ,  $K_g = 1.3$ ). The left arrow corresponds to the monitoring velocity, and the right arrow to the control flow velocity.

over the S5 panel (Fig. 12 (b)) and further to the rear body (S6) (Fig. 12 (c)). The expanded vortex is released in the next time without merging to the large-scale vortex which has appeared in the case without flow control (Fig. 4 (c)). The reason for this is that the flow control regulates the vortex generation and periodical vortex shedding prevents vortices to merge into the large-scale vortex causing the high drag.

Figure 13 compares the average pressure distribution along the surface between the results with and without flow control. It reveals that the drag reduction due to the feedback flow control is ascribed to the increase in pressure on the panel S7. By referring to the former result in

Fig. 5 where the pressure distribution at the high-drag instant shows substantially small pressure on the panel S7, the increase in average pressure there is the result of the feedback flow control that prevents the occurrence of the high-drag flow pattern.

Since the feedback control consumes energy for the control input, it is crucial to evaluate the balance between the power saved by drag reduction and that consumed by the flow control. Figure 14 shows the power consumption for the cases with and without control. As shown in the left bar, the power consumption due to drag without control is 35 000 W. The power consumption due to drag with control is 27 000 W and that for the flow control is 280 W.

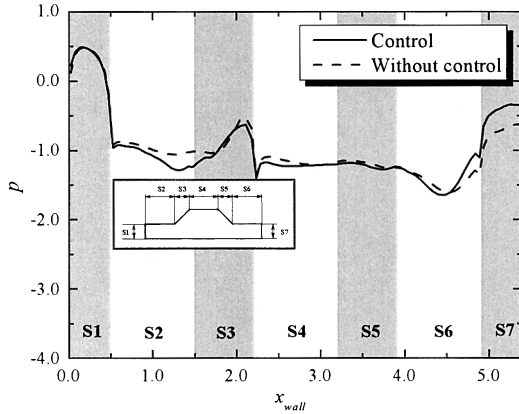


Fig. 13 Pressure distribution with and without control

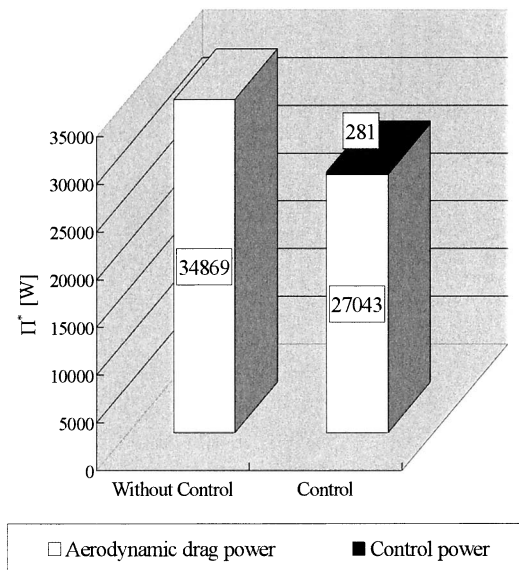


Fig. 14 Comparison of power consumption

Power saving of 8 000 W resulting from the feedback flow control is much larger than the power needed for the control, and overall power saving of 21% is attained by the present feedback flow control.

**4. Conclusion**

As the fundamental study of aerodynamic drag reduction for a vehicle with a feedback flow control, two-dimensional calculation was performed for a flow around a simplified vehicle model. The mechanism of unsteady drag was explained in relation to the vortex shedding from the model. The location of the control flow nozzle was so determined that the control flow influences the drag most effectively. Based on the physical consideration of the drag generation, the location of the output velocity mea-

surement was changed over a limited region near the front windshield. A systematic calculation revealed that the output signal defined in a small region results in a significant drag reduction of 20% from the case without control. The present feedback flow control is generally applicable to the drag reduction of the bluff body for which the drag is generated with the same mechanism of essentially two-dimensional vortex shedding.

**References**

- (1) Janssen, L.J. and Emmelmann, H.-J., Aerodynamic Improvements—A Great Potential for Better Fuel Economy, SAE Paper No.780265, (1978), pp.1261–1269.
- (2) Lay, W.E., Is 50 Miles Per Gallon Possible with Correct Streamlining?, SAE-Journal, Vol.32, No.4 (1933), pp.144–156.
- (3) Hucho, W.H., Janssen, L.T. and Emmelmann, H.J., The Optimization of Body Details—A Method for Reducing the Aerodynamic Drag of Road Vehicles, SAE Paper No.760185, (1976), pp.865–882.
- (4) Bearman, P.W., Some Observations on Road Vehicle Wakes, SAE Paper No.840301, (1984), pp.504–515.
- (5) Gad-el-Hak, M., Flow Control, (2000), Cambridge University Press.
- (6) Choi, H., Moin, P. and Kim, J., Active Turbulence Control for Drag Reduction in Wall-Bounded Flows, Journal of Fluid Mechanics, Vol.262 (1994), pp.75–110.
- (7) Lumley, J. and Blossey, P., Control of Turbulence, Annual Review of Fluid Mechanics, Vol.30 (1998), pp.311–327.
- (8) Bewley, T., Teman, R. and Ziane, M., A General Framework for Robust Control in Fluid Mechanics, Physica D, Vol.138, No.(3-4) (2000), pp.360–392.
- (9) Brogan, W.L., Modern Control Theory, Third Edition, (1991), Prentice-Hall.
- (10) Ahmed, S.R., Ramm, G. and Faltin, G., Some Salient Features of the Time-Averaged Ground Vehicle Wake, SAE Paper No.840300, (1984), pp.473–503.
- (11) Nisugi, K., Hayase, T. and Shirai, A., Aerodynamic Drag Reduction by Feedback Control of Flow Field, Proceedings of Sixth Triennial International Symposium on Fluid Control, Measurement and Visualization, (2000), CD-ROM.
- (12) Patankar, S.V., Numerical Heat Transfer and Fluid Flow, (1980), Hemisphere.
- (13) Hayase, T., Humphrey, J.A.C. and Greif, R., A Consistently Formulated QUICK Scheme for Fast and Stable Convergence Using Finite-Volume Iterative Calculation Procedures, Journal of Computational Physics, Vol.98 (1992), pp.108–118.
- (14) Fletcher, C.A.J., Computational Techniques for Fluid Dynamics, Vol.1, (1988), Springer-Verlag.